Dynamics of colloids in confined geometries

2011 J. Phys.: Condens. Matter 23 184115

(http://iopscience.iop.org/0953-8984/23/18/184115)

IOP Publishing Journal of Physics: Condensed Matter

J. Phys.: Condens. Matter **23** (2011) 184115 (9pp) doi:10.1088/0953-8984/23/18/184115

Dynamics of colloids in confined geometries

L Almenar and M Rauscher

Max-Planck-Institut für Metallforschung, Heisenbergstraße 3, D-70569 Stuttgart, Germany
and
Institut für Theoretische und Angewandte Physik, Universität Stuttgart, Pfaffenwaldring 57, D-70569 Stuttgart, Germany

E-mail: rauscher@mf.mpg.de

Received 31 May 2010
Published 20 April 2011
Online at stacks.iop.org/JPhysCM/23/184115

Abstract

We discuss the Brownian dynamics of colloids in confinement with special emphasis on the influence of the solvent dynamics. We review the derivation of a dynamic density functional theory (DDFT) including some aspects of hydrodynamic interactions and its application to the micro-rheology of suspensions. In particular we discuss the failure of Stokes' law in suspensions and non-equilibrium solvent structure mediated interactions. With regard to hydrodynamic chromatography we also discuss the stationary transport of particles in narrow channels, and the reasons for the failure of DDFT in this situation.

(Some figures in this article are in colour only in the electronic version)

1. Introduction

Colloidal suspensions have received a lot of attention because of their ubiquity in nature and because of their technological relevance. The mutual interactions between suspended particles can be tuned in many ways, e.g., by adding salts, by changing the pH-level, or by adding a depletion agent such as colloidal particles or polymers. Since the equilibrium properties of matter do not depend on the underlying dynamics but only on the interactions among the constituent particles, colloidal suspensions are a versatile model system for studying the equilibrium phase behavior of condensed matter (as long as quantum effects do not play a role) [1].

However, out of equilibrium, dynamics does matter. While most simple fluids (with molecular sizes in the Angstrom range) are very well described by hydrodynamic equations down to the nanometer scale (if the finite range of intermolecular forces, thermal fluctuations, and hydrodynamic slip are taken into account [2]) the hydrodynamic description of colloidal suspensions already breaks down at the micron scale. For example, in the vicinity of solid surfaces one can observe depletion layers with a reduced solute density or even oscillations of the solute density as a function of the distance from the wall. This depletion layer does influence the flow of the suspension along the surface, in particular it can result in a significant apparent hydrodynamic slip, since the viscosity in the depletion layer is smaller than the viscosity of the bulk suspension [3, 4]. In thin capillaries, wall effects lead to a purely hydrodynamic separation of suspended particles by size. This phenomenon is used in hydrodynamic chromatography in order to analyze the composition of polydisperse mixtures [5–8]. Because the solvent molecules can flow into and out of the depletion layer, suspended particles can be moved from one side of a channel to the other side by wall structures such as bumps [9, 10], they accumulate in front of moving objects [11–14] and therefore increase their friction over the value expected from, e.g., Stokes law for spheres [15], and reduce their diffusivity [16].

The challenges in understanding the non-equilibrium dynamics of confined colloidal suspensions are on the one hand to bridge the length and timescales involved in the problem, ranging from the scale of the solvent molecules to the size of a microfluidic device. However, it turns out that scales can be separated rather efficiently in this type of system. On the other hand, colloidal systems are much more complex than simple fluids in the sense that they are much less well defined, e.g., there is usually a significant polydispersity, and the surface charge on the colloids, which determines the strength of the electrostatic interactions, is hard to measure and varies from colloid to colloid.

With this in mind we aim for qualitative rather than quantitative understanding of the dynamics of colloidal

suspensions in confinement. We focus on three paradigmatic situations in particular: the micro-rheology of suspensions, non-equilibrium entropic forces, and transport in the vicinity of walls and in narrow channels. The latter is motivated by its application for hydrodynamic chromatography [5].

In section 2 we review the Brownian dynamics of colloidal suspensions in confinement, and in section 3 we summarize the developments of the classical dynamic density functional theory (DDFT) in recent years. In section 4 we apply the DDFT to the micro-rheology of suspensions and to non-equilibrium entropic forces. In section 5 we discuss the transport of suspensions in narrow channels. We close with a summary and an outlook in section 6.

2. Brownian dynamics

The relevant length scale in suspensions is the particle size, which is in the micron regime. However, as compared to the molecular dynamics in simple fluids, colloids are rather slow. The diffusion time R^2/D (with the diffusion constant $D = k_\mathrm{B}T\gamma$ and the Stokes mobility $\gamma = 1/(6\pi\eta R)$ in a medium of viscosity η), i.e., the time it takes a colloid in water ($\eta \approx 10^{-3}$ N s m^{-2}) at room temperature T to diffuse across its own radius R, is on the order of seconds.

The large difference in time and length scales between the solvent molecules and the colloids allows one to treat the solvent as a continuum modeled by hydrodynamic equations, in the simplest case by the incompressible Stokes equation. Thermal fluctuations have to be taken into account, either in terms of a stochastic hydrodynamic equation or in terms of a random fluctuation force acting on the colloidal particles. Both approaches are equivalent as long as fluctuation induced forces are negligible. In simple fluids this is the case far from critical points (e.g., at the end of the liquid–vapor coexistence line or in phase-separating binary mixtures) where the critical Casimir force becomes a relevant factor [17, 18].

By integrating out solvent degrees of freedom in this way, one is left with the Brownian dynamics of the suspended particles. Inertia effects can be safely ignored for suspended colloids: the velocity relaxation time $m\gamma$ for micron sized particles is in the sub-microsecond regime, i.e., much shorter than the diffusion time. In this limit, dynamics of an ensemble of N identical particles[1] at positions $\mathbf{r}_i(t)$, $i = 1, \ldots, N$, in an external force field $\mathbf{G}(\mathbf{r}) = -\nabla U(\mathbf{r})$ and with pairwise interactions forces $\mathbf{F}(\mathbf{r}) = -\nabla\Phi(\mathbf{r})$ is given by the following set of stochastic differential equations [19]:

$$\frac{\mathrm{d}\mathbf{r}_i}{\mathrm{d}t} = \mathbf{u}(\mathbf{r}) + \frac{R^2}{6}\nabla^2\mathbf{u}(\mathbf{r}) + \boldsymbol{\gamma}(\mathbf{r}_i)\cdot\left[\mathbf{G}(\mathbf{r}_i) + \sum_{j=1}^{N}\mathbf{F}(\mathbf{r}_i - \mathbf{r}_j)\right] + \sqrt{k_\mathrm{B}T\boldsymbol{\gamma}(\mathbf{r}_i)}\cdot\mathbf{N}_i(t). \quad (1)$$

The first two terms on the right-hand side are the Faxén drift velocity $\mathbf{u}^*(\mathbf{r}) = \mathbf{u}(\mathbf{r}) + \frac{R^2}{6}\nabla^2\mathbf{u}(\mathbf{r})$ of a particle of finite radius R in an inhomogeneous solvent flow field $\mathbf{u}(\mathbf{r})$ [20]. The next term is the product of the sum of all forces acting on particle i (in square brackets) multiplied by the position dependent 3×3-mobility tensor $\boldsymbol{\gamma}(\mathbf{r}_i)$. In a bulk system, the mobility is a number given by Stokes law, but in the vicinity of confining surfaces, the mobility depends on the direction relative to the surface and on the distance from the surface [21, 22]. The last term is the random thermal velocity generated by the chaotic motion of the solvent molecules. The Gaussian white noise $\mathbf{N}_i(t)$ has zero mean $\langle\mathbf{N}_i(t)\rangle = 0$ and the correlator is given by

$$\langle\mathbf{N}_i(t)\otimes\mathbf{N}_j(t')\rangle = 2\mathbf{1}\delta_{ij}\delta(t-t'). \quad (2)$$

The pre-factor of the noise term in equation (1) is determined by the fluctuation dissipation theorem: in equilibrium (which implies $\mathbf{u} = 0$) the probability density P_eq to find the particles at positions $\{\mathbf{r}_\ell\}$ has to be given by the Boltzmann distribution

$$P_\mathrm{eq}(\{\mathbf{r}_\ell\}) = \mathcal{Z}^{-1}\exp\left\{-\frac{1}{k_\mathrm{B}T}\sum_{i=1}^{N}\left[\sum_{j=1}^{N}\Phi(\mathbf{r}_i-\mathbf{r}_j) + V(\mathbf{r}_i)\right]\right\}, \quad (3)$$

which is normalized by the partition sum $\mathcal{Z}$. Since the pre-factor to $\mathbf{N}_i$ in equation (1) depends on the position of the particle i, i.e., the noise is multiplicative, one has to specify the stochastic calculus [23, 24]. In the case of equation (1), one arrives at the proper Fokker–Planck equation for the time evolution of the probability density $P(\{\mathbf{r}_\ell\}, t)$ in the Klimontovich calculus [25, 26], see also [27] and references therein,

$$\partial_t P(\{\mathbf{r}_\ell\},t) + \sum_{i=1}^{N}\nabla_i\cdot\left[\mathbf{u}^*(\mathbf{r}_i)P(\{\mathbf{r}_\ell\},t)\right] = -\sum_{i=1}^{N}\nabla_i\cdot\left\{\boldsymbol{\gamma}(\mathbf{r}_i)\cdot\left[\sum_{j=1}^{N}\mathbf{F}(\mathbf{r}_i-\mathbf{r}_j) + \mathbf{G}(\mathbf{r}_i) - k_\mathrm{B}T\nabla_i\right]\times P(\{\mathbf{r}_\ell\},t)\right\}, \quad (4)$$

with $\nabla_i = \frac{\partial}{\partial\mathbf{r}_i}$. One could also choose a different calculus (e.g., Ito or Stratonovich), but then the Langevin equation (1) has to be modified by adding an extra drift term [28]. As pointed out in [19], this complication is an artifact of the over-damped limit; the under-damped dynamics is perfectly well defined.

Hydrodynamic interactions among the suspended particles can be included in terms of a $3N\times3N$-mobility tensor which depends on all particle positions. On the Rotne–Prager level the sub-matrices coupling the motion of particle i and j only depend on their relative distance but not on the positions of other particles [29, 30]. However, the Rotne–Prager approach is only valid in bulk situations. In the vicinity of walls and surfaces, hydrodynamic interactions are screened and become shorter ranged as compared to the bulk. For example, their leading order dependence on the distance r between the particles is $1/r^2$ rather than $1/r$ in bulk [31]. To date the Rotne–Prager approach has not been generalized to inhomogeneous situations and, although in bulk hydrodynamic interactions among particles are known to be of great importance (e.g., they are responsible for the enhanced viscosity of dilute suspensions and their reduced sedimentation

[1] The generalization to two or more component systems is straightforward, however, for simplicity of notation we only discuss one-component systems in sections 2 and 3.

rate as compared to that of an isolated particle), their reduced range in confinement might render them less important. For this reason we will not consider hydrodynamic interactions among particles explicitly in the following.

In Brownian dynamics simulations, equation (1) is solved numerically. With a typical size in the micron range, there are on the order of 10^9 particles in a mm^3 of solution, which is the typical volume of interest in microfluidic devices. This number is much smaller than the number of molecules which one has to consider in a molecular dynamics simulation of fluidic systems, and the relevant timescales are much longer. For this reason, Brownian dynamics simulations have turned out to be a rather powerful simulation tool for complex fluids. However, obtaining good statistics is still computationally demanding and within simulations one cannot bridge the scale towards macroscopic systems seamlessly, e.g., in order to obtain particle scale resolution only in the vicinity of container walls. Here, a continuum method describing the dynamics of ensemble averaged quantities is needed. One such method is the DDFT which will be presented in the following.

3. Dynamic density functional theory

The DDFT is a non-equilibrium version of the classical density functional theory (DFT) for equilibrium systems, as described, e.g., in [32–34]. DFT has significantly contributed to the understanding of the inhomogeneous structure of confined fluids on the length scale of the constituent particles. Within this approach, the equilibrium particle density distribution $\rho_{\mathrm{eq}}(\mathbf{r})$ in a grand canonical system of volume $\mathcal{V}$ is obtained from a rigorous variation principle: it minimizes the grand canonical free energy functional. For one-component systems it has the following form:

$$\Omega[\rho] = \mathcal{F}[\rho] - \int_{\mathcal{V}} \rho(\mathbf{r})\mu \, \mathrm{d}^3 r, \tag{5}$$

with the chemical potential μ. The Helmholtz free energy functional

$$\mathcal{F}[\rho] = \int_{\mathcal{V}} \rho(\mathbf{r}) \left[k_{\mathrm{B}}T \ln \lambda^3 \rho(\mathbf{r}) - 1 + U(\mathbf{r})\right] \mathrm{d}^3 r + \mathcal{F}_{\mathrm{ex}}[\rho], \tag{6}$$

is the sum of the ideal-gas part ($\lambda = \sqrt{h^2/(2k_{\mathrm{B}}T\pi m)}$ is the thermal de Broglie wavelength) and the excess free energy $\mathcal{F}_{\mathrm{ex}}[\rho]$ which results from the interactions among the particles. With the exception of some one-dimensional systems, $\mathcal{F}_{\mathrm{ex}}[\rho]$ is not known exactly, but approximate functionals are available for a large class of systems. Quadratic functionals have been used successfully for soft and weakly interacting systems, and functionals based on fundamental measure theory for hard sphere systems [35]. Weak long ranged interactions on top of hard core repulsion have been treated perturbatively.

One can also prove the existence of a DDFT for classical systems [36]. As in the static case, the proof is non-constructive, and at the moment there is no DDFT for simple fluids available—not even for ideal systems. However, for over-damped Brownian particles, Marconi and Tarazona have developed a successful DDFT for the time evolution of the *ensemble averaged* density $\rho(\mathbf{r}, t)$ [37, 38]. By construction this DDFT is deterministic, in contrast to a theory for coarse grained densities, see [39]. Español and Löwen present an alternative derivation based on projection operator techniques in [40].

Originally, the DDFT was developed for Brownian particles but in the absence of hydrodynamic effects, i.e., without an advecting flow field and without hydrodynamic interactions of any kind: the mobility is a position independent scalar. In the following, we review the derivation of this DDFT and the implications of having an advecting field and a position dependent mobility tensor $\boldsymbol{\gamma}(\mathbf{r})$, which is presented in more detail in [41, 19]. The starting point is equation (4). By integrating this equation over all but one of the particle positions, one obtains a time evolution equation for the ensemble averaged particle density $\rho(\mathbf{r}, t)$ [42]. The resulting time evolution equation for $\rho(\mathbf{r}, t)$ depends on $\rho(\mathbf{r}, t)$ and the non-equilibrium two-body distribution function $\rho^{(2)}(\mathbf{r}, \mathbf{r}', t)$:

$$\begin{aligned}
&\partial_t \rho(\mathbf{r}, t) + \nabla \cdot \left[\mathbf{u}^*(\mathbf{r})\rho(\mathbf{r}, t)\right] \\
&= \nabla \cdot \left(\boldsymbol{\gamma}(\mathbf{r}) \cdot \left\{ [k_{\mathrm{B}}T\nabla - \mathbf{G}(\mathbf{r})]\rho(\mathbf{r}, t) \right.\right. \\
&\quad \left.\left. - \int_{\mathcal{V}} \rho^{(2)}(\mathbf{r}, \mathbf{r}', t)\mathbf{F}(\mathbf{r} - \mathbf{r}') \, \mathrm{d}^3 r' \right\} \right).
\end{aligned} \tag{7}$$

This time evolution equation for $\rho(\mathbf{r}, t)$ is the lowest member in a hierarchy of N equations that is similar to the Bogoliubov–Born–Green–Kirkwood–Yvon (BBGKY) hierarchy for simple fluids [39, 34, 42–44]. The DDFT is obtained by using a closure relation to truncate this hierarchy: the non-equilibrium two-body distribution function $\rho^{(2)}(\mathbf{r}, \mathbf{r}', t)$ is approximated by the corresponding correlations in an equilibrium system with the same one-body density distribution. For $\mathbf{u}(\mathbf{r}) = \boldsymbol{b}$ one can show that for any system (specified by $\Phi(\mathbf{r})$, $U(\mathbf{r})$, N, and T) with a given density distribution $\rho(\mathbf{r})$ there is a unique additional external potential $V_\rho(\mathbf{r})$, such that the system would be in equilibrium if it was exposed to this potential. Approximating the correlation function in the last term in equation (7) with the correlation function $\rho^{(2)}_{\mathrm{eq}}(\mathbf{r}, \mathbf{r}')$ in the corresponding equilibrium system one can identify this term with the gradient of the first direct correlation function $c^{(1)}_{\mathrm{eq}}(\mathbf{r})$, i.e., the variational derivative of the excess part of the free energy functional with respect to $\rho(\mathbf{r})$:

$$\begin{aligned}
&\int_{\mathcal{V}} \rho^{(2)}_{\mathrm{eq}}(\mathbf{r}, \mathbf{r}')\mathbf{F}(\mathbf{r} - \mathbf{r}') \, \mathrm{d}^3 r' = k_{\mathrm{B}}T\rho(\mathbf{r}, t)\nabla c^{(1)}_{\mathrm{eq}}(\mathbf{r}) \\
&= -\rho(\mathbf{r}, t)\nabla \left. \frac{\delta \mathcal{F}_{\mathrm{ex}}[\rho]}{\delta \rho(\mathbf{r})} \right|_{\rho(\mathbf{r},t)}.
\end{aligned} \tag{8}$$

If $\boldsymbol{\gamma}^{-1}(\mathbf{r}) \cdot \mathbf{u}^*(\mathbf{r})$ is rotation free one can find a potential $U^*(\mathbf{r})$ such that $\boldsymbol{\gamma}^{-1}(\mathbf{r}) \cdot \mathbf{u}^*(\mathbf{r}) = -\nabla U^*(\mathbf{r})$. The system is then formally equivalent to a system without flow field but in an external potential $U(\mathbf{r}) + U^*(\mathbf{r})$ [14, 19]. In this case one gets

$$\begin{aligned}
&\partial_t \rho(\mathbf{r}, t) + \nabla \cdot [\mathbf{u}^*(\mathbf{r})\rho(\mathbf{r}, t)] \\
&= \nabla \cdot \left[\boldsymbol{\gamma}(\mathbf{r})\rho(\mathbf{r}, t) \cdot \nabla \left. \frac{\delta \mathcal{F}[\rho]}{\delta \rho} \right|_{\rho(\mathbf{r},t)} \right].
\end{aligned} \tag{9}$$

Flows with $\nabla \times (\boldsymbol{\gamma}^{-1} \cdot \mathbf{u}^*) \neq \mathbf{0}$ represent an external drive for the system which does not allow the system to equilibrate: the

stationary probability density $P(\{\mathbf{r}_\ell\})$ does not fulfill detailed balance. However, external potentials or potential flows do not enter the closure relation in equation (8) and it is tempting to use it even for non-potential flows. This leads to equation (9), which one would also get by a phenomenological approach to include advection into DDFT.

In this section and in section 4 we restrict ourselves to one-component systems with pairwise interactions between the particles. Many-body interactions, which means that the interaction potential between two particles depends on the positions of other particles, do not lead to any complications in the derivation of the DDFT. With many-body interactions, the right-hand side of equation (7) depends not only on the pair distribution function but also on higher distribution functions. However, with the same equilibrium assumption used above, the sum of all the terms appearing on the right-hand side due to direct interactions can be approximated by $-\rho(\mathbf{r},t)\nabla\frac{\delta\mathcal{F}_{\rm ex}[\rho]}{\delta\rho(\mathbf{r})}|_{\rho(\mathbf{r},t)}$ such that the final DDFT is again given by equation (9) [42].

And the generalization to mixtures is straightforward in the Brownian dynamics equation (1) and in the corresponding Fokker–Planck equation (4): the radius R, the mobility tensor $\boldsymbol{\gamma}$ as well as the forces $\mathbf{G}$ and $\mathbf{F}$ depend on the particle type (or the types of interacting particles in the case of $\mathbf{F}$). One obtains equations of motion for the density $\rho_\nu(\mathbf{r},t)$ of particle type ν by integrating out all degrees of freedom apart from the position of one particle of type ν. Using the same type of closure relation discussed above, one gets [44]

$$\partial_t\rho_\nu(\mathbf{r},t)+\nabla\cdot\left[\mathbf{u}^*_\nu(\mathbf{r})\rho_\nu(\mathbf{r},t)\right] = \nabla\cdot\left[\boldsymbol{\gamma}_\nu(\mathbf{r})\rho_\nu(\mathbf{r},t)\cdot\nabla\frac{\delta\mathcal{F}[\rho_1\rho_2\cdots]}{\delta\rho_\nu(\mathbf{r})}\bigg|_{\rho_1(\mathbf{r},t),\rho_2(\mathbf{r},t)\cdots}\right]. \quad (10)$$

The Faxén drift velocity $\mathbf{u}^*_\nu$ depends on the particle type via the particle radius R_ν.

Up to this point we have ignored hydrodynamic interactions among the particles. On the Rotne–Prager level, they enter the Brownian dynamics via a $3N\times 3N$-dimensional mobility tensor which couples the motions of the particles pairwise [29, 30]. In the case of a one-component system with pairwise interactions, integrating out the corresponding Fokker–Planck equation over $N-1$ particle positions leads to an evolution equation for the density which depends on the two-body and on the three-body correlation functions. Two-body correlations are generated either by direct or hydrodynamic pair-interactions, and three-particle correlations are found between three particles, of which one is coupled hydrodynamically to one particle and directly to another one [45, 46]. Nevertheless, a local equilibrium approximation for the many-body distribution functions can be used to develop a DDFT [47, 48]. However, in contrast to the correlations generated by direct interactions, the correlations induced by hydrodynamic interactions cannot be directly written in terms of the variation of the free energy. These must be calculated from direct correlation functions (i.e., variations of the free energy functional) via Ornstein–Zernike relations. The resulting DDFT equation is less elegant than the ones presented here, but the results are very promising. In particular, the agreement with Brownian dynamics simulations is greatly improved as compared to equation (9). On a phenomenological level, one aspect of hydrodynamic interactions, namely the reduced mobility of the particles in dense systems, can be taken into account in terms of a density dependent mobility $\boldsymbol{\gamma}(\rho(\mathbf{r},t),\mathbf{r})$ [49]. However, a density dependent mobility cannot be incorporated consistently into the Brownian dynamics.

4. Micro-rheology of suspensions

As mentioned in the introduction, one of the main consequences of the large difference in size between the solvent molecules and the suspended colloids is that the solvent molecules can get much closer to any confining surface than the colloids. This is also true for any obstacle moving through a suspension, e.g., a spherical particle. Therefore one expects particles to accumulate in front of the obstacle, i.e., it should act as a rake. In the absence of a solvent (or, equivalently, assuming that the obstacle is transparent for the solvent) the resulting density distributions around the obstacle have been discussed in detail for non-interacting particles at arbitrary Péclet numbers [13] and for interacting particles at finite Péclet numbers [11]. In both cases there is a bow wave of particles in front of the obstacle in which the density is enhanced and a wake behind the obstacle. However, in a suspension the solvent has to flow around the obstacles, which generates a long ranged flow field in which the suspended particles are advected away from the obstacle. For an incompressible Newtonian solvent at low Reynolds numbers this flow field can be calculated analytically and one gets in a frame of reference co-moving with the obstacle [50]

$$\mathbf{u}(\mathbf{r}) = \frac{3A}{4r}\left(1+\frac{A^2}{3r^2}\right)\mathbf{v}+\frac{3A}{4r^3}\mathbf{r}(\mathbf{r}\cdot\mathbf{v})\left(1-\frac{A^2}{r^2}\right)-\mathbf{v}, \quad (11)$$

with the obstacle radius and velocity, A and $\mathbf{v}$, respectively. Figure 1 shows the flow field around a sphere of radius A moving in the positive x-direction. The closest point a suspended particle can get to the sphere surface is indicated. Clearly, the flow field has a non-zero normal component to this surface in front of and behind the sphere. This normal component goes to zero as the size of the advected particles vanishes. In this limit the advected particles behave like solvent molecules and there is no accumulation of particles in front of the obstacle. For vanishing obstacle size we recover the case studied in [11, 13]: the flow field is undisturbed by the obstacle, i.e., $\mathbf{u}(\mathbf{r})=-\mathbf{v}$, and the bow wave is maximal [14].

This bow wave and the wake have two major effects. On the one hand they increase the friction of particles moving though a suspension. The inhomogeneous density distribution around the obstacle results in an inhomogeneous pressure and therefore in a net force opposing the direction of motion. In the case of ideal particles the pressure of the suspended particles is proportional to their local density. The resulting force is simply given by the integral of the pressure over the obstacle surface $-\int_{\partial O}k_{\rm B}T\rho(\mathbf{r},t)\hat{\mathbf{n}}\cdot{\rm d}^2\mathbf{A}$, with the outward pointing surface normal vector $\hat{\mathbf{n}}$. Combining Brownian dynamics (BD) simulations and a very simple DDFT calculation (essentially neglecting interactions between the suspended particles) we

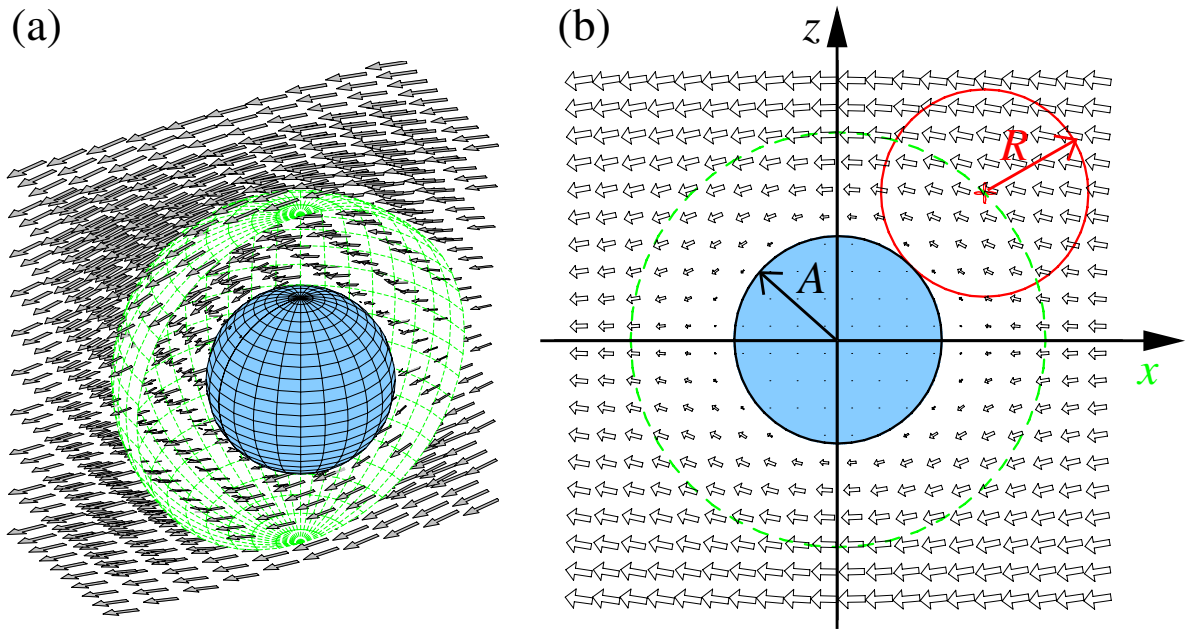

Figure 1. Flow field (arrows) of an incompressible Newtonian fluid around a sphere of radius A (full blue) moving in a positive x-direction in the co-moving frame of reference. The points closest to the sphere that the centers of mass of advected particles of radius R (red/full line open circle in (b)) can get to are indicated in dashed green. (a) A partially cut-open 3D view and (b) a cut in the x–z-plane. Note that the flow field inside the dashed green sphere/circle is non-zero.

have been able to show that this force, which adds to the viscous Stokes drag, explains the drag force on a colloidal particle dragged through a solution of λ-DNA using an optical tweezer [15]. However, a quantitative DDFT model of the experimental system would have to account for the interactions among the λ-DNA coils. Also, both the BD simulations and the numerical solution of the DDFT are limited to rather small Péclet numbers, i.e., rather small speeds $\mathbf{v}$ of the obstacle, while the experiments had to be performed at rather large velocities. Ignoring the interactions between the particles leads to a diverging contact density at the obstacle for $|\mathbf{v}| \to \infty$ which causes numerical instabilities. Taking into account interactions would limit the contact density, but it would lead to a bow wave with a spatial extent that grows with the velocity $|\mathbf{v}|$, as seen in lattice gas models [51–53]. The bow wave induced friction also leads to a reduced diffusivity of the suspended particles [16].

A second effect of the bow wave and the wake near the moving particle is that a second particle in its vicinity feels an inhomogeneous environment which leads to a net force acting on it [12, 54]. Solvent structure mediated forces can also be observed in equilibrium: the confinement of the fluid, e.g., due to the presence of two spherical particles, leads to density variations in their vicinity, which, in turn, lead to forces between the particles. An over-simplified (neglecting the mutual interaction between the second species) but intuitive picture has been given by Asakura and Oosawa [55]: each large colloid is surrounded by a depletion layer which has a width equal to the radius of the second particle type, and which cannot be entered by the centers of mass of the second species due to steric hindrance. If the two large particles come sufficiently close together so that these depletion layers overlap, the total excluded volume is reduced. In this way, the available volume for the second (smaller) species increases, which leads to an increase of the entropy. The resulting entropic force is therefore attractive. Evidence for this force is provided by the phase diagram of colloid–polymer mixtures, which cannot be understood without this entropic interaction, see [56] and references therein, as well as by direct measurements, see [57] for example. Non-spherical particles will also experience a torque which is expected to play a role in enzymatic reactions, see [58]. If the direct interactions between particles are short ranged, the ranges of equilibrium depletion forces are short as well, in general comparable to the size of the constituent particles. But the range of the non-equilibrium fluid structure mediated forces are long. As a result, even if their distance is large as compared to their size, two spheres moving in parallel repel each other due to the accumulation of suspended particles in-between. This is also the case for a sphere moving in parallel to a wall. And two tailgating spheres attract each other. However, for symmetry reasons these interactions vanish to linear order in the Péclet number: the same is true for hydrodynamic interactions in this configuration, but with the relevant number being the Reynolds number rather than the Péclet number. As a consequence one can expect to observe fluid structure mediated forces in total absence of hydrodynamic interactions. In contrast to slipstreaming road cyclists, at low Péclet numbers both spheres experience a reduced drag as compared to an isolated sphere [54]. However, in this study the effect of hydrodynamic interactions was not considered.

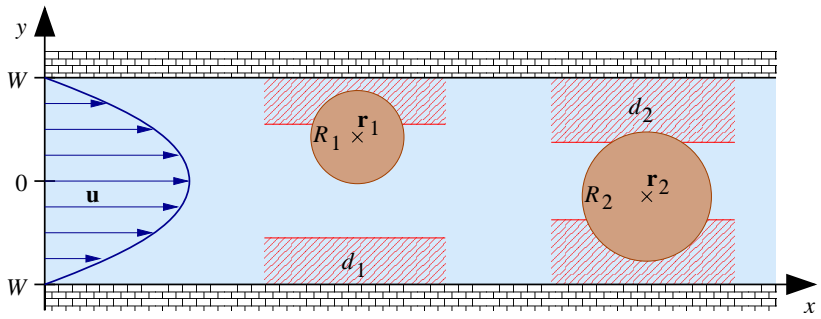

Figure 2. 2D model system for the transport of a polydisperse mixture in a narrow channel. Two particles at $\mathbf{r}_1$ and $\mathbf{r}_2$, respectively, are advected in a Poiseuille flow with the maximal flow velocity u_0 at $y = 0$. The interaction between the particles is either hard core with a minimal distance $d = R_1 + R_2$ or soft with a Gaussian potential mimicking the interaction among polymer coils. The interaction with the wall can be either hard such that the hatched areas are unaccessible to the particles, or soft, mimicking the interaction of polymers with solid walls.

5. Suspensions and in channels

The heterogeneity in complex fluids induced by streaming past obstacles in channels has also been suggested as a means to sort particles and to separate solute and solvent in a suspension [10]. However, in homogeneous straight channels and at flat walls the stationary solutions of the DDFT equations (9) and (10) are trivial: the solvent flow field is parallel to the (channel) wall (e.g., in the x-direction) and the magnitude of the flow field as well as the stationary solutions only depend on the direction normal to the channel wall (e.g., on y). As a consequence, equations (9) and (10) are solved by the equilibrium distributions $\frac{\delta\mathcal{F}[\rho]}{\delta\rho} = \mu = \text{const.}$ and $\frac{\delta\mathcal{F}[\rho_1,\rho_2,\ldots]}{\delta\rho_i} = \mu_i = \text{const.}$, respectively [59]. Neither taking into account direct interactions among the particles nor hydrodynamic interactions between the particles and the wall changes this result. However, as shown below, the density distribution as well as the correlations within a channel are changed by flow. The reason for this failure of DDFT is the equilibrium closure for the correlation function in equation (7) which explicitly fixes the correlations to their equilibrium values.

This can be demonstrated in a simple 2D model for hydrodynamic chromatography [5–8], illustrated in figure 2: two interacting particles advected by $\mathbf{u}(y) = u(y)\hat{\mathbf{e}}_x = u_0[1 - (y/W)^2]\hat{\mathbf{e}}_x$ in a 2D channel of width $2W$ and length L with periodic boundary conditions in the x-direction. The interactions among the particles can be either hard core, with a minimum distance d between the particle centers of mass, or soft, with a Gaussian potential $\Phi(r) = \Phi_0 \exp(-r^2/d^2)$ mimicking the interaction among polymer coils in a good solvent. The interaction of the particles with the walls is also either hard, such that the particles are confined to a strip of with $2W_{1/2} = 2(W - d_{1/2})$ in the center of the channel, or soft (again mimicking the entropic repulsion of a polymer from a solid wall in a rather crude way), with wall potentials $V_{1/2}(y) = V_{01/02}[\frac{W^2}{(y-W)^2} + \frac{W^2}{(y+W)^2} - 1]$. In order to relate this to the results obtained with hard potentials we choose the potential strengths $V_{01/02}$ such that $V_{1/2}(\pm W_{1/2}) = k_\mathrm{B}T$. We have not considered electrostatic effects at this point, but we do not expect details of the shape of the potential to change our findings in a qualitative way [60].

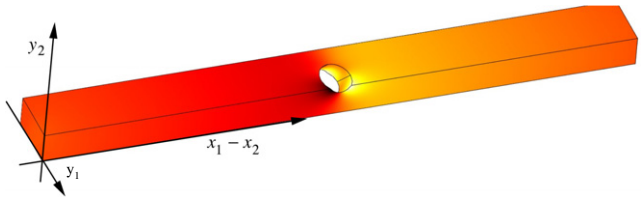

Figure 3. Stationary solution $P(x_2 - x_1, y_1, y_2)$ of equation (12) for Péclet number $Pe = 1$, $L = 20W$, $W_1 = W$, and $W_2 = 0.5W$. The direction and position independent mobilities of the two particles are taken to be equal. The gray scale/colors encode the value of P on the boundaries of the domain ranging from 0.025 317 (dark red/black) to 0.026 106 (bright yellow/white). P is normalized to 1.

With $\Psi(\mathbf{r}_1, \mathbf{r}_2) = V_1(y_1) + V_2(y_2) + \Phi(|\mathbf{r}_2 - \mathbf{r}_1|)$ the Fokker–Planck equation for the probability density $P(\mathbf{r}_1, \mathbf{r}_2, t)$ corresponding to the Brownian dynamics of the two particles is given by

$$\begin{aligned}\partial_t P + u(y_1)\partial_{x_1} P + u(y_2)\partial_{x_2} P \\ = \nabla_1 \cdot \boldsymbol{\gamma}_1 \cdot (k_\mathrm{B}T\nabla_1 P + P\nabla_1\Psi) \\ + \nabla_2 \cdot \boldsymbol{\gamma}_2 \cdot (k_\mathrm{B}T\nabla_2 P + P\nabla_2\Psi).\end{aligned} \tag{12}$$

Equation (12) can be written in terms of a conservation law $\partial_t W + \nabla_1 \cdot \mathbf{j}_1 + \nabla_2 \cdot \mathbf{j}_2 = 0$ with the probability current densities

$$\mathbf{j}_{1/2}(\mathbf{r}_1, \mathbf{r}_2, t) = \mathbf{u}(\mathbf{r}_{1/2})P - \boldsymbol{\gamma}_{1/2} \cdot (k_\mathrm{B}T\nabla_{1/2}P + P\nabla_{1/2}\Psi). \tag{13}$$

In particular we are looking for stationary solutions of equation (12) which depend only on y_1, y_2, and $x_2 - x_1$. In this case, equation (12) can be written as a stationary drift-diffusion problem in three spatial dimensions, which can be solved with standard numerical methods. We use the finite element software FEMLAB.

For hard interaction potentials, the stationary problem further reduces to an advection-diffusion problem in a channel of length L, width $2W_1$, and height $2W_2$, which is intersected by an elliptic cylinder with the half axes d and $d/\sqrt{2}$ centered about the diagonal of the y_1–y_2-plane [59]. Figure 3 shows the solution of the drift-diffusion problem for Péclet number $Pe = \frac{u_0 W}{D_{1/2}} = 1$, $L = 20W$, $W_1 = W$, and $W_2 = 0.5W$. For this example, the mobilities are assumed to be position and direction independent and equal for both particles.

Therefore the corresponding diffusion constants $D_{1/2} = k_B T \gamma_{1/2}$ are equal and the system is described by only one Péclet number. The intersecting cylinder is clearly visible as well as the heterogeneities in its vicinity. With hydrodynamic chromatography in mind, we calculate the throughputs

$$Q_{1/2} = \frac{1}{L} \int j_{x_{1/2}}(\mathbf{r}_1, \mathbf{r}_2)\, \mathrm{d}^2 r_1\, \mathrm{d}^2 r_2 \tag{14}$$

of the two particles through the channel as a function of d_1, d_2, d, and u_0 (i.e., the Péclet number Pe). Figure 4(a) shows the fluxes Q_1 and Q_2 as a function of d_1 and d_2 for $L = 20$, $d = 1/\sqrt{2}$, and $Pe = 1$. As expected, the fluxes are equal for $d_1 = d_2$, i.e., if the particles are identical, and if $d_1 + d_2 + d > 2W$, i.e., if the particles cannot pass each other. The flux of the larger particle is bigger: $Q_1 < Q_2$ for $d_1 < d_2$ and vice versa. The reason is simply that the larger particles only sample the high solvent flow region in the channel center while the smaller ones also spend time next to the channel wall where the flow velocity is much smaller[2]. The difference in throughput between particles of different size decreases with increasing interaction radius d, as shown in figure 4(b): the bigger particle drags the smaller one along and the smaller one hinders the bigger one.

We also calculate the probability density distributions $\bar{\rho}_{1/2}(y)$ for finding particle 1 or 2, respectively, at a certain vertical position y in the channel

$$\bar{\rho}_1(y_1) = \int P(\mathbf{r}_1, \mathbf{r}_2)\, \mathrm{d}x_1\, \mathrm{d}x_2\, \mathrm{d}y_2 \qquad \text{and}$$
$$\bar{\rho}_2(y_2) = \int P(\mathbf{r}_1, \mathbf{r}_2)\, \mathrm{d}x_1\, \mathrm{d}x_2\, \mathrm{d}y_1. \tag{15}$$

Without interactions between the particles (i.e., for $d = 0W$) we have $\bar{\rho}_{1/2} = 1/(2W_{1/2})$ for $|y| < W_{1/2}$ and zero for $|y| > W_{1/2}$. Due to the hard core repulsion between the particles, the density of the smaller particle is significantly reduced in the channel center, while the density of the larger particle is less affected, as shown in figure 5(a). With the smaller particles being pushed towards the channel wall, one might assume that interactions among the particles enhance the difference between their throughputs. But this is only the case if one ignores the diffusive current and the drift current (second term on the right-hand side of equation (13)). As shown in figure 4(b), interactions do reduce the difference in throughput.

In the absence of interactions the throughputs $Q_{1/2}$ are strictly linear in the Péclet number since $P(\mathbf{r}_1, \mathbf{r}_2)$ is independent of Pe. This is not the case for finite d: as shown in figure 5(a) the larger particles are slightly concentrated in the channel center and the smaller ones are even more pushed towards the wall for increasing Péclet numbers. As a result, the throughput of the smaller particles increases less than linearly with Pe, see figure 5(b). If the particles are so large that they cannot pass each other, their throughput is equal but it also increases less than linearly with the Péclet number.

Up to this point we have neglected hydrodynamic interactions with the channel walls and we have assumed the mobilities to be equal. We have tested the influence of hydrodynamic interactions with the channel walls and we also did calculations with different mobilities but we did not observe any qualitative changes.

While for hard particles the only relevant parameters are the Péclet number Pe and the three lengths $d_{1/2}/W$ and d/W, the situation is different for soft particles. There, the dimensionless potential strength $\Phi_0/(k_B T)$ is a fifth relevant parameter—the wall potential strengths $V_{01/02}$ can be related to the lengths $d_{1/2}$. For hard particles, one only distinguishes between small Péclet numbers $Pe \ll 1$, for which diffusion dominates over advection, and large Péclet numbers $Pe \gg 1$, for which advection dominates. For soft particles, in addition one has to distinguish between weak and strong interaction potentials. However, at this point only preliminary results are available, mainly because of numerical issues related to the divergence of the wall potentials $V_{1/2}$. But preliminary calculations with hard wall potentials indicate that the probability densities $\bar{\rho}_{1/2}(y)$ become independent of Pe for $Pe \gg 1$ and $Pe \gg \Phi_0/(k_B T)$.

[2] A large hydrodynamic slip would lead to a plug flow with $\mathbf{u}$ only weakly depending on y. Hydrodynamic chromatography would not work in such a system.

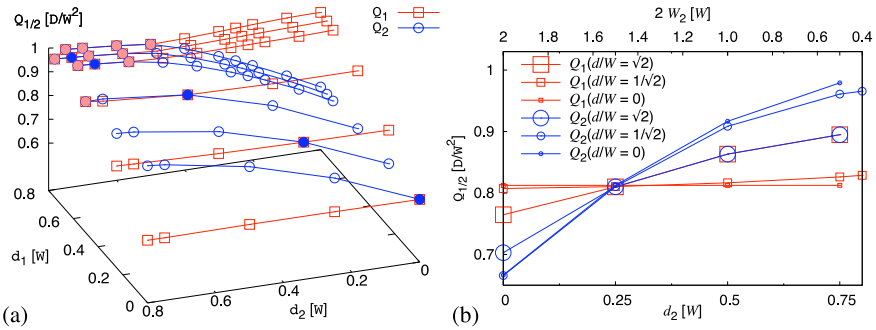

Figure 4. Throughputs Q_1 (red squares) and Q_2 (blue circles) of the two particles, respectively. (a) Throughputs as a function of d_1 and d_2 for $Pe = 1$, $L = 20$, and $d = W/\sqrt{2}$. Filled symbols indicate values of d_1 and d_2 for which the fluxes are equal, either because d_1 and d_2 are equal (dark blue symbols) or because the particles cannot pass each other (light red symbols). (b) Throughputs as a function of d_2 for $d_1 = 0.25W$, $Pe = 1$, $L = 20$, and $d/W = 0, 1/\sqrt{2}$, and $\sqrt{2}$. For $d_2 > 0.336W$ and $d/W = \sqrt{2}$ the particles cannot pass each other. For $d/W = 1/\sqrt{2}$ this happens for $d_2 > 1.04W$ (not on the graph). The mobilities are assumed equal and scalar (i.e., hydrodynamic interactions with the walls are ignored here).

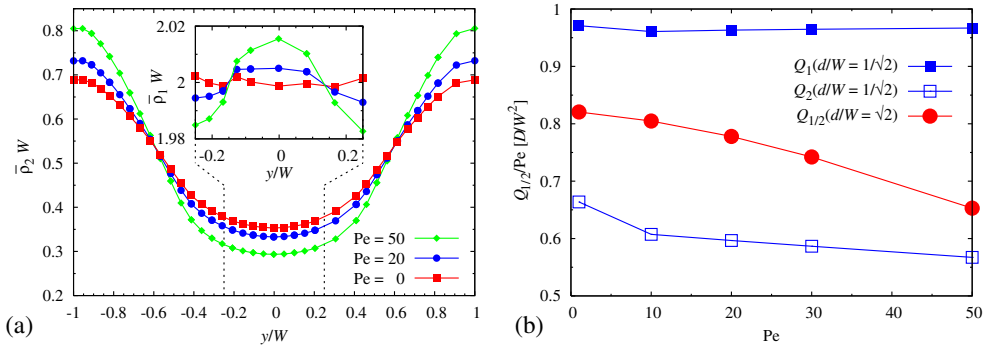

Figure 5. (a) The probability densities $\bar{\rho}_{1/2}(y)$ to find the bigger particle 1 ($d_1 = 0.75W$; inset) and the smaller particle 2 ($d_2 = 0W$; main figure) at a certain value y in a channel of length $L = 4W$ for $d = \sqrt{0.5}W$ and Péclet numbers $Pe = 0$, 20, and 50. Dashed lines indicate the size of the blowup region. Without interactions ($d = 0W$) the densities would be $\rho_1 = 2/W$ and $\rho_2 = 1/(2W)$. (b) The throughputs of particle 1 ($d_1 = 0.25W$) and 2 ($d_2 = 0W$) normalized to the Péclet number as a function of Pe. For $d = W/\sqrt{0.5}$ (filled and open squares $L = 4W$) the two particles can still pass each other, but for $d = \sqrt{2}W$ (circles, $L = 10W$) they cannot. As in (a), $d_1 = 0.75W$ and $d_2 = 0W$. Mobilities are assumed to be equal, scalar, and position independent.

6. Summary and outlook

The dynamics of confined suspensions remains a challenging field for theoretical descriptions but it has great relevance for practical applications such as hydrodynamic chromatography [5–8]. DDFT is one of the few theoretical approaches which allows for a particle scale resolution at places where it is needed, e.g., in the vicinity of walls or in narrow channels, but which smoothly connects to macroscopic bulk dynamics. In the bulk where the density is almost constant, the last term on the right-hand side of equation (7) is negligible. In this limit equation (9) reduces to the simple drift-diffusion equation expected for macroscopic systems. DDFT has therefore a great potential to bridge the large gap of length scales between the particle scale and the macroscopic scale. In addition, in the absence of a flow field $\mathbf{u} = \mathbf{0}$, one can show that within DDFT the system relaxes towards the equilibrium density distribution given by the free energy functional used for the dynamics: under DDFT dynamics the total free energy in the system never increases [14].

We have used the DDFT rather successfully to model the micro-rheology of solutions. The friction force on colloidal particles moving through a solution is larger than the Stokes friction, even considering the bulk viscosity of the solution. The reason for this is the accumulation of particles in front of the colloid and the reduced particle density just behind the colloid [15]. This non-equilibrium density distribution also reduces the diffusivity of colloids in solutions significantly [16].

However, DDFT fails when it comes to dense non-equilibrium steady states as discussed in section 5. The primary reason is the local equilibrium closure for the two-point correlations in equation (8). The probability density $P(\mathbf{r}_1, \mathbf{r}_2, t)$ discussed in section 5 is the two-point correlation function for a system of exactly two particles. And from the stationary solutions of equation (12) it is evident that the correlations differ significantly from the equilibrium correlations. Closing the hierarchy (of which equation (7) is the first equation) at the next order, i.e., an equilibrium closure relation for the three-point correlation function, might help. But it would lead to a set of equations for the density and the two-point correlation function, i.e., to a much higher dimensional problem. Equilibrium density functional theory is a grand canonical theory but the BD is conserved: particle exchange between the system and a reservoir is only possible through boundaries. However, we still use grand canonical functionals for the DDFT. This might be an additional source of error.

For these reasons, we resorted to a simple two-dimensional two-particle system in order to get insight into the transport of colloidal suspensions in thin channels. The objective was to assess the influence of interactions among the particles, and between the particles and the channel walls on the particle separation in hydrodynamic chromatography. While hydrodynamic interactions between the particles and the wall seem to have little influence on the particle transport, we could show that separation is hindered by direct interactions among the particles but increased by higher flow velocities.

Apart from the problems related to the local equilibrium closure in DDFT, the two main challenges for modeling the dynamics of confined suspensions are hydrodynamic interactions among particles and to obtain quantitative results. There has been a significant and rather successful effort to include hydrodynamic interactions among particles into DDFT. However, the Rotne–Prager approach taken in [47, 48] is limited to bulk systems, and in the vicinity of solid surfaces hydrodynamic interactions are strongly modified [31]. It is not clear whether hydrodynamic interactions can be treated as pairwise as in the Rotne–Prager approximation. And while bulk properties of suspensions are rather well characterized, there is a large polydispersity in size and surface charge. In particular, the latter one is important in order to understand the interactions of an individual particle with a solid surface. We have analyzed the BD of individual particles near a wall [61], but we were unable to directly relate this to the results of double focus fluorescence correlation spectroscopy measurements (see, e.g., [62]) due to the lack of quantitative information on the system.

The local equilibrium closure used in the derivation of DDFT is problematic in stationary non-equilibrium situations.

However, DDFT can model relaxing systems rather accurately, see for example [37, 63, 47, 48]. For such systems, it is a rather valuable theoretical tool for understanding the dynamics of confined suspensions. Inspired by recent advances in the theoretical understanding of size selectivity in biological ion channels [64], we have used DDFT to model the transient behavior of local demixing in binary mixtures [44]. These results cannot be related directly to the actual dynamics in biological ion channels since the sizes of the ions and the solvent molecules (i.e., water) are not well separated. A DDFT for simple fluids as suggested by [36] is needed here—another great challenge for the future.

Acknowledgments

We acknowledge financial support within the priority program 'Nano and Microfluidics' SPP 1164 of the Deutsche Forschungsgemeinschaft. We enjoyed many inspiring and fruitful discussions with Jens Harting, Friedrich Kremer, Artur Straube, and Olga Vinogradova (in alphabetical order).

References

[1] Hansen J P and McDonald I R 1990 *Theory of Simple Liquids* 2nd edn (New York: Academic)
[2] Rauscher M and Dietrich S 2008 *Annu. Rev. Mater. Res.* **38** 143–72
[3] Tuinier R and Taniguchi T 2005 *J. Phys.: Condens. Matter* **17** L9–14
[4] Tuinier R, Dhont J K G and Fan T H 2006 *Europhys. Lett.* **75** 929–35
[5] Tijssen R, Bleumer J P A and Van Kreveld M E 1983 *J. Chromatogr.* A **260** 297–304
[6] Tijssen R, Bos J and Van Kreveld M E 1986 *Anal. Chem.* **58** 3036–44
[7] Stegeman G, van Asten A C, Kraak J C, Poppe H and Tijssen R 1994 *Anal. Chem.* **66** 1147–60
[8] Blom M T, Chmela E, Gardeniers J G E, Tijssen R, Elwenspoek M and van den Berg A 2002 *Sensors Actuators* B **82** 111–6
[9] Schindler M 2006 Free-surface microflows and particle transport *PhD Thesis* Universität Augsburg
[10] Schindler M, Talkner P, Kostur M and Hänggi P 2007 *Physica* A **385** 46–58
[11] Penna F, Dzubiella J and Tarazona P 2003 *Phys. Rev.* E **68** 061407
[12] Dzubiella J, Löwen H and Likos C N 2003 *Phys. Rev. Lett.* **91** 248301
[13] Squires T M and Brady J F 2005 *Phys. Fluids* **17** 073101
[14] Rauscher M, Krüger M, Dominguez A and Penna F 2007 *J. Chem. Phys.* **127** 244906
[15] Gutsche C, Kremer F, Krüger M, Rauscher M, Weeber R and Harting J 2008 *J. Chem. Phys.* **129** 084902
[16] Krüger M and Rauscher M 2009 *J. Chem. Phys.* **131** 094902
[17] Fisher M E and de Gennes P G 1978 *C. R. Acad. Sci., Ser.* B **287** 207–9
[18] Krech M 1994 *The Casimir Effect in Critical Systems* (Singapore: World Scientific)
[19] Rauscher M 2010 *J. Phys.: Condens. Matter* **22** 364109
[20] Faxén H 1922 *Ann. Phys., Lpz.* **373** 89–119
[21] Happel J and Brenner H 1965 *Low Reynolds Number Hydrodynamics* (Englewood Cliffs, NJ: Prentice-Hall)
[22] Lauga E and Squires T M 2005 *Phys. Fluids* **17** 103102
[23] Gardiner C W 1983 *Handbook of Stochastic Methods for Physics, Chemistry and the Natural Sciences* (*Springer Series in Synergetics* vol 13) 1st edn (Berlin: Springer)
[24] Risken H 1984 *The Fokker–Planck Equation* (*Springer Series in Synergetics* vol 18) (Berlin: Springer)
[25] Klimontovich Y L 1994 *Phys.—Usp.* **37** 737–66
[26] Dunkel J, Hilbert S and Hänggi P 2006 *Irreversible Prozesseund Selbstorganisation* ed L Schimansky-Geier, H Malchow and T Pöschel (Berlin: Logos) pp 11–21
[27] Dhont J K G 1996 *J. Chem. Phys.* **105** 5112–25
[28] van Kampen N G 1981 *J. Stat. Phys.* **24** 175–87
[29] Rotne J and Prager S 1969 *J. Chem. Phys.* **50** 4831–7
[30] Jeffrey D J and Onishi Y 1984 *J. Fluid Mech.* **139** 261–90
[31] Dufresne E R, Squires T M, Brenner M P and Grier D G 2000 *Phys. Rev. Lett.* **85** 3317–20
[32] Evans R 1979 *Adv. Phys.* **28** 143–200
[33] Evans R 1992 *Fundamentals of Inhomogeneous Fluids* ed D Henderson (New York: Dekker) chapter 3, pp 85–173
[34] Hansen J P and McDonald I R 2006 *Theory of Simple Liquids* 3rd edn (New York: Academic)
[35] Roth R 2010 *J. Phys.: Condens. Matter* **22** 063102
[36] Chan G K L and Finken R 2005 *Phys. Rev. Lett.* **94** 183001
[37] Marconi U M B and Tarazona P 1999 *J. Chem. Phys.* **110** 8032–44
[38] Marconi U M B and Tarazona P 2000 *J. Phys.: Condens. Matter* **12** A413–8
[39] Archer A J and Rauscher M 2004 *J. Phys. A: Math. Gen.* **37** 9325–33
[40] Español P and Löwen H 2009 *J. Chem. Phys.* **131** 244101
[41] Rauscher M 2008 *Encyclopedia of Microfluidics and Nanofluidics* vol 2, ed D Li (New York: Springer) pp 428–33
[42] Archer A J 2005 *J. Phys.: Condens. Matter* **17** 1405–27
[43] Archer A 2009 *J. Chem. Phys.* **130** 014509
[44] Roth R, Rauscher M and Archer A J 2009 *Phys. Rev.* E **80** 021409
[45] Harris S 1976 *J. Phys. A: Math. Gen.* **9** 1895–8
[46] Felderhof B U 1978 *J. Phys. A: Math. Gen.* **11** 929–37
[47] Rex M and Löwen H 2008 *Phys. Rev. Lett.* **101** 148302
[48] Rex M and Löwen H 2009 *Eur. Phys. J.* E **28** 139–46
[49] Royall C P, Dzubiella J, Schmidt M and van Blaaderen A 2007 *Phys. Rev. Lett.* **98** 188304
[50] Landau L D and Lifshitz E M 2005 *Fluid Mechanics* (*Course of Theoretical Physics* vol 6) 2nd edn (Amsterdam: Elsevier) (Heidelberg: Butterworth-Heinemann)
[51] Bénichou O, Cazabat A M, Coninck J D, Moreau M and Oshanin G 2000 *Phys. Rev. Lett.* **84** 511–4
[52] Bénichou O, Cazabat A M, Coninck J D, Moreau M and Oshanin G 2001 *Phys. Rev.* B **63** 235413
[53] Oshanin G, Bénichou O, Burlatsky S F and Moreau M 2004 *Instabilities and Non-Equilibrium Structures* vol 9, ed O Descalzi, J Marténez and S Rica (Dordrecht: Kluwer) pp 33–74
[54] Krüger M and Rauscher M 2007 *J. Chem. Phys.* **127** 034905
[55] Oosawa F and Asakura S 1954 *J. Chem. Phys.* **22** 1255–6
[56] Likos C N 2001 *Phys. Rep.* **348** 267–439
[57] Helden L, Roth R, Koenderink G H, Leiderer P and Bechinger C 2003 *Phys. Rev. Lett.* **90** 048301
[58] Roth R, van Roij R, Andrienko D, Mecke K R and Dietrich S 2002 *Phys. Rev. Lett.* **89** 088301
[59] Almenar L and Rauscher M 2011 in preparation
[60] Almenar L 2011 *PhD Thesis* Universität Stuttgart (expected)
[61] Almenar L 2007 Brownian dynamics in near surface flows *Master's Thesis* Universität Stuttgart
[62] Vinogradova O I, Koynov K, Best A and Feuillebois F 2009 *Phys. Rev. Lett.* **102** 118302
[63] Rex M, Likos C N, Löwen H and Dzubiella J 2006 *Mol. Phys.* **104** 527–40
[64] Roth R and Gillespie D 2005 *Phys. Rev. Lett.* **95** 247801